

## Surface ozone climatology of South Eastern Brazil and the impact of biomass burning events

Targino, Admir Crésó; Harrison, Roy M.; Krecl, Patricia; Glantz, Paul; de Lima, Caroline Hatada; Beddows, David

DOI:

[10.1016/j.jenvman.2019.109645](https://doi.org/10.1016/j.jenvman.2019.109645)

License:

Creative Commons: Attribution-NonCommercial-NoDerivs (CC BY-NC-ND)

*Document Version*

Peer reviewed version

*Citation for published version (Harvard):*

Targino, AC, Harrison, RM, Krecl, P, Glantz, P, de Lima, CH & Beddows, D 2019, 'Surface ozone climatology of South Eastern Brazil and the impact of biomass burning events', *Journal of Environmental Management*, vol. 252, 109645. <https://doi.org/10.1016/j.jenvman.2019.109645>

[Link to publication on Research at Birmingham portal](#)

### **Publisher Rights Statement:**

Checked for eligibility: 06/11/19.

Published by Elsevier in Journal of Environmental Management: <https://doi.org/10.1016/j.jenvman.2019.109645>

### **General rights**

Unless a licence is specified above, all rights (including copyright and moral rights) in this document are retained by the authors and/or the copyright holders. The express permission of the copyright holder must be obtained for any use of this material other than for purposes permitted by law.

- Users may freely distribute the URL that is used to identify this publication.
- Users may download and/or print one copy of the publication from the University of Birmingham research portal for the purpose of private study or non-commercial research.
- User may use extracts from the document in line with the concept of 'fair dealing' under the Copyright, Designs and Patents Act 1988 (?)
- Users may not further distribute the material nor use it for the purposes of commercial gain.

Where a licence is displayed above, please note the terms and conditions of the licence govern your use of this document.

When citing, please reference the published version.

### **Take down policy**

While the University of Birmingham exercises care and attention in making items available there are rare occasions when an item has been uploaded in error or has been deemed to be commercially or otherwise sensitive.

If you believe that this is the case for this document, please contact [UBIRA@lists.bham.ac.uk](mailto:UBIRA@lists.bham.ac.uk) providing details and we will remove access to the work immediately and investigate.

Surface ozone climatology of South Eastern Brazil and the impact of biomass burning  
events

Admir Créso Targino<sup>a,†,\*</sup>, Roy M. Harrison<sup>b,††</sup>, Patricia Krecl<sup>a</sup>, Paul Glantz<sup>c</sup>

Caroline Hatada de Lima<sup>a,†</sup>, David Beddows<sup>b</sup>

<sup>a</sup>Graduate Program in Environmental Engineering, Federal University of Technology,  
Av. Pioneiros 3131, 86036-370, Londrina, PR, Brazil

<sup>b</sup>School of Geography, Earth and Environmental Sciences, University of Birmingham,  
Edgbaston, Birmingham, B15 2TT, United Kingdom

<sup>c</sup>Department of Environmental Science and Analytical Chemistry, Stockholm  
University, Svante Arrhenius väg 8, 106 91, Stockholm, Sweden

<sup>†</sup>Also at: Graduate Program in Geography, Londrina State University, Rod. Celso  
Garcia, Km 380, 86057-970, Londrina, PR, Brazil

<sup>††</sup> Also at: Department of Environmental Sciences, Centre of Excellence in  
Environmental Studies, King Abdulaziz University, PO Box 80203, Jeddah, 21589,  
Saudi Arabia.

\*Corresponding author: admirtargino@utfpr.edu.br

## Abstract

In the austral spring, biomass fires affect a vast area of South America each year. We combined *in situ* ozone ( $O_3$ ) data, measured in the states of São Paulo and Paraná, Brazil, in the period 2014-2017, with aerosol optical depth, co-pollutants ( $NO_x$ ,  $PM_{2.5}$  and  $PM_{10}$ ) and air backtrajectories to identify sources, transport and geographical patterns in the air pollution data. We applied cluster analysis to hourly  $O_3$  data and split the investigation area of approximately 290,000 km<sup>2</sup> into five groups with similar features in terms of diurnal, weekly, monthly and seasonal  $O_3$  concentrations. All groups presented a peak in September and October, associated with the fire activities and enhanced photochemistry. The highest mean  $O_3$  concentrations were measured inland whilst, besides having lower concentrations, the coastal group was also associated with the smallest diurnal and seasonal variations. The latter was attributed to lower photochemical activity due to frequently occurring overcast weather situation. The mean annual regional contribution of  $O_3$  over the area was 61  $\mu\text{g}/\text{m}^3$ , with large seasonal and intersite variabilities (from 35 to 84  $\mu\text{g}/\text{m}^3$ ). The long-range transport of smoke contributed with between 23 and 41% of the total  $O_3$  during the pollution events. A pollution outbreak in September 2015 caused many-fold increases in  $O_3$ ,  $PM_{2.5}$  and  $PM_{10}$  across the investigation area, which exceeded the World Health Organisation recommendations. We show that the regional transport of particulates and gas due to biomass burning overlays the local emissions in already highly polluted cities. Such an effect can outweigh local measures to curb anthropogenic air pollution in cities.

Key words: Short-lived climate forcer; Transboundary pollution; Cluster analysis; Air quality

## 1. Introduction

Planet Earth is frequently affected by smoke from fires caused by humans (*e.g.*, burning of vegetation and waste, preparation of agriculture fields, conversion of cropland to pasture) and by natural processes (*e.g.*, lightning-induced fires). Australia, California and many other regions of Earth are prone to wildfires, defined as uncontrollable fires caused by the concomitant occurrence of vegetative resources to burn (such as forest, shrub or grass), sustained dry spells and ignition sources. Wildfires are seasonal because the constraints for their occurrence (especially fire-conducive weather patterns) occur in specific periods of the year (Krawchuk *et al.*, 2009). Fires that particularly take place at low temperatures and limited oxygen favour the formation of trace gases, such as VOC, CO and NO<sub>x</sub> (NO+NO<sub>2</sub>), and particulate matter (PM<sub>2.5</sub>, PM<sub>10</sub> and black carbon) (Akagi *et al.*, 2011; Wevers *et al.*, 2004; Crutzen and Andreae, 1990). The transboundary transport of smoke from wildfires and agricultural burns deteriorates the air quality downstream of the burning areas (McClure and Jaffe, 2018a; Targino and Krecl, 2016; Sarangi *et al.*, 2014; Sillanpää *et al.*, 2005), even at a considerable distances from the sources (over 2,000 km, see Targino *et al.*, 2013 and Witham and Manning, 2007).

One aggravating aspect about wildfires is that they are becoming longer and more frequent in some regions of the planet, such as Eurasia and western North America (Riaño *et al.*, 2007), which may be related to anthropogenic climate change (Flannigan *et al.*, 2013; 2009). For South America, Riaño *et al.* (2007) showed a consistent fire regime of interannual cycles with no clear trends for any month or annually. The majority of wildfires in Brazil occurs in the dry season (between July and September) in the areas of Amazon, Cerrado (a savanna-like biome of central Brazil) and in the Pampas (grasslands in Southern Brazil). In the Amazon and Cerrado, the wildfires are predominantly man-made, with the purpose of removing brush, accumulated waste and vegetation to install

crop cultures or pastures (Ten Hoeve *et al.*, 2012; Pivello, 2011). Moreover, sugar cane field burning to eliminate the sharp-edged leaves and poisonous animals before harvesting also contributes to regional biomass smoke (Allen *et al.*, 2004).

Depending on the meteorological setting, the long-range transport of smoke during the dry season affects the air quality of small and large cities downwind of the fire spots, including the megacity of São Paulo (e.g., Lopes *et al.*, 2012; Freitas *et al.*, 2005; Reinhardt, 2001). Freitas *et al.* (2005) observed that the position of the South Atlantic subtropical high pressure plays an important role in the transport of aerosol plumes from the Amazon region to Southern Brazil. This system also prevents rain-bearing cold fronts from penetrating the area, favouring the accumulation of pollutants and deterioration of the air quality (Oliveira *et al.*, 2016; Targino and Krecl, 2016).

The hotspot of primary pollutants is found at the fire front, whilst high concentrations of secondary pollutants, such as tropospheric ozone ( $O_3$ ) are usually detected a few kilometres downwind of the burning area (Wentworth *et al.*, 2018).  $O_3$  is formed via a series of complex, non-linear reactions involving  $NO_x$  and non-methane VOC in the presence of sunlight (Monks *et al.*, 2015 and references therein). The  $O_3$  production rate is governed by  $NO_x$ - or VOC-limited conditions and possibly aerosol effects on the photochemical production (Baylon *et al.*, 2018; Alvarado *et al.*, 2015).

Many countries have targeted the transportation sector as a strategy for abating air pollution and global warming. For example, in 2015, the mayors of eight Latin American cities (Curitiba, Rio de Janeiro, Salvador, Bogotá, Quito, Caracas, Buenos Aires and Mexico City) members of C40 –a network of the world’s megacities committed to tackle climate change ([www.c40.org](http://www.c40.org))– signed a declaration of intent in which 35% of the diesel-fuelled public buses will be replaced by hybrid and electric buses by 2020. Although this is an important measure to tackle air pollution in cities, they may not be enough if other

sources prevail, such as biomass burning. McClure and Jaffe (2018a) reported maximum daily (8-h average) O<sub>3</sub> increase up to 70 µg/m<sup>3</sup> on days affected by smoke in Meridian (USA). Zhou *et al.* (2019) observed a concomitant 2.5-fold increase in O<sub>3</sub> concentrations at three sites in the Sichuan Basin (China) due to biomass burning, whilst Lin *et al.* (2013) reported an increase from 200 ppb to 600 ppb at Mei-Feng (Taiwan) due to the outflow of smoke from South East Asia. Besides affecting air quality and increasing the risk of death from respiratory causes (Jerrett *et al.*, 2009), O<sub>3</sub> is a short-lived climate forcer (residence time of the order of several weeks in the free-troposphere, Monks *et al.*, 2015). Hence, mitigating O<sub>3</sub> levels has two-fold benefits: reducing the impacts on air quality and climate.

Atmospheric emission data for Brazil are rare and reliable emission inventories remain elusive. However, the NO<sub>x</sub> and non-methane hydrocarbons (NMHC) estimates from biomass burning and the road transport sectors provided by the EDGAR v4.2 database (Crippa *et al.*, 2018) reveal the importance of biomass burning for atmospheric chemistry. The NO<sub>x</sub> emissions from savanna, agricultural waste, forest and grassland fires in 2008 were 434.14 Gg whilst the road transport sector emitted 1,270 Gg. In terms of NMHC, the figures are 839.4 and 1,250 Gg, respectively. However, considering that the fires in Brazil occur mainly over three months, the emissions from the road transport should be scaled accordingly to make a fair comparison. If we divide the annual road transport NO<sub>x</sub> and NMHC emissions by four, we obtain 317.5 and 312.5 Gg, respectively, over three months, which suggests that emissions from biomass burning make up a substantial fraction of the precursors for O<sub>3</sub> formation.

In this study, we present a four-year climatology of O<sub>3</sub> for the states of São Paulo and Paraná (Brazil), using ground-based *in situ* observations. We quantify the contribution of long-range transport on the O<sub>3</sub> concentration in cities of different sizes by analysing the

coupling between O<sub>3</sub>, NO and NO<sub>2</sub>. We assess the impact of long-range transported smoke from central Brazil on the air quality by investigating a pollution outbreak within the most polluted months of 2015. We analysed the *in situ* data in combination with co-pollutants (NO<sub>x</sub>, PM<sub>2.5</sub> and PM<sub>10</sub>), satellite retrieved aerosol optical depth, fire spots and airmass backward trajectories.

## **2. Methodology and data analysis**

### **2.1 Study area**

São Paulo is one of the 27 Brazilian federal units, located in the South Eastern region. It is the wealthiest and most populous state, accounting for 33.9% of the country's total GDP (Gandhi *et al.*, 2017) and hosting approximately one fifth of the country's population (45 million inhabitants). The state of São Paulo's economy is diversified and the chemical, sugar and ethanol production, metalworking, machinery, automobile and aviation industries account for 75% of the economic sector (Governo do Estado de São Paulo, 2019). The state has the largest vehicular fleet in the country, with 28.6 million units (DENATRAN, 2018) that emitted 331, 180, 5 and 4.7 Gg of CO, NO<sub>x</sub>, PM and SO<sub>2</sub>, respectively, in 2016. About 60% of these emissions occurred in the municipalities that form the metropolitan area of São Paulo (MASP), the cities of Campinas, Sorocaba, and urban agglomerations in Baixada Santista and Vale do Paraíba (CETESB, 2017). The vehicular emissions of NO<sub>x</sub> and total hydrocarbons (THC) dominate at state level (65 and 87%, respectively) and in the MASP (75 and 87%, respectively), which emphasises the effect this sector may have on local air quality.

### **2.2 Data**

We used a combination of ground-based *in-situ*, remote sensing and modelling data to investigate the O<sub>3</sub> climatology at sites in the states of São Paulo and Paraná from 2014 to 2017. The *in situ* data are from 25 sites managed by São Paulo State Environmental Company (CETESB) and from Londrina, a mid-sized city located in the neighbouring state of Paraná (Fig. 2). The CETESB monitors criteria air pollutant with methods that follow closely those of the US Environmental Protection Agency. The data from Londrina were collected at the campus of the Federal University of Technology (UTFPR). A full list of the cities included in this study is provided in Table S1 (Supplementary Material). Note that Brazilian air quality networks are not designed for remote or rural conditions, like the sites in Europe (*e.g.*, Targino *et al.*, 2013; Witham and Manning, 2007). Instead, they are located in the urban core, close to highly-trafficked streets or industrial areas. This means that the analysis of long-range transport of air pollutants is more challenging, since the regional contribution cannot be easily isolated from local urban contributions. The MODerate resolution Imaging Spectroradiometer (MODIS) Aqua and Terra Collection 6.1 Level 2 standard 10-km products were used here for best quality retrievals (quality flag = 3) of aerosol optical depth (AOD) over land. The data were obtained through NASA Goddard Space Flight Center's Atmosphere Archive and Distribution System (<http://ladsweb.nascom.nasa.gov>). Detailed descriptions of the MODIS dark target algorithm for retrievals of AOD over land can be found in Levy *et al.* (2013; 2007). Fire spots were identified by satellite remote sensing furnished by the National Space Research Institute of Brazil (<http://www.inpe.br/queimadas/bdqueimadas>) (INPE, 2018). Infrared radiation at 3.7 and 4.1  $\mu\text{m}$  emitted from the fires is detected by the Advanced very-high-resolution radiometer (AVHRR) on board the polar-orbit satellites NOAA-15, NOAA-18, NOAA-19 and METOP-B, MODIS on board TERRA and AQUA, VIIRS on board NPP-Suomi and the geostationary satellites GOES-13 and MSG-3. The product



identifies spots at least 30 m long, occurring on non-cloudy days and with fire outbreaks lasting long enough to be captured between images.

To assess influences of atmospheric large-scale circulation on the air quality at the sites, five-day backward trajectories that arrived at 500 m above terrain level were calculated with 1-hour interval, eight times per day (00, 03, 06, 09, 12, 15, 18, 21 h), using the Hybrid Single Particle Lagrangian Integrated Trajectory Model (HYSPLIT) (Stein *et al.*, 2015). ERA-Interim reanalysis data of diagnosed boundary layer height, with three-hour time resolution, was taken from the European Centre for Medium-Range Weather Forecasts (ECMWF). We use meteorological data (air temperature, relative humidity, solar irradiance, wind speed and direction and atmospheric pressure) measured at UTFPR campus and at CETESB sites.

### **2.3 Cluster analysis**

We applied hierarchical cluster analysis to reduce the number of observations and to find groups of similar stations within the O<sub>3</sub> dataset. We used O<sub>3</sub> concentrations due to the large data availability and its relatively long residence time in the atmosphere, which makes it a good tracer of long-range transported pollution. This technique was successfully used by Lyapina *et al.* (2016) to classify surface O<sub>3</sub> data over 1,400 European monitoring stations.

The hourly O<sub>3</sub> concentration for 26 sites in the period 2014-2017 yielded a matrix of 34,560 rows and 26 columns. The hierarchical clustering procedure starts with each site in its own group, which is progressively merged with the most similar site until all sites are in a single group. Observations that are as homogeneous as possible are collected into a group (large intra-group similarity), whilst keeping between-group (inter-group) observations as heterogeneous as possible (Hair *et al.*, 1998).

We used Ward's minimum variance method as merging criterion, since it has been widely used for climatic classifications with superior performance compared to other methods (*e.g.*, Kalkstein and Corrigan, 1986). Ward's method starts with  $K$  groups (in our case,  $K$  sites) and at each step it fuses groups based on an error function that leads to a minimal within-group sum of squared distances ( $W$ ) between the points and the centroids of the merged groups (Wilks, 2011). This means that the pair to be merged must minimise the sum of the squared distances between the data points and the centroids of their respective groups, summed over the resulting groups (Wilks, 2011):

$$W = \sum_{k=1}^K \sum_{j=1}^J \sum_{i=1}^N (x_{ijk} - \bar{x}_{jk})^2, \quad 1$$

where  $x_{ijk}$  is the  $i$ -th  $O_3$  concentration of the  $j$ -th site in the  $k$ -th group,  $J$  is the number of sites,  $N$  the number of observations, and  $\bar{x}_{jk}$  is the mean  $O_3$  concentration inside this group. Ward's method computes  $W$  and  $W'$  before and after the merging, respectively, and merges clusters with the smallest  $\Delta W = W' - W$ .

We applied two approaches to decide on the number of clusters: the elbow and silhouette methods. The elbow method consists in running the clustering algorithm for a range of number of clusters ( $n$ ) and calculating  $W$  for each  $n$ .  $W$  decreases monotonically as the number of  $n$  increases, and the  $W$  vs.  $n$  plot usually shows a bend which can be taken as a cut-off point to determine the number of clusters. From that point on, the  $W$  decrease flattens, indicating small changes and exaggerated specificity in the choice of clusters by increasing  $n$  (Lyapina *et al.*, 2016). The silhouette method (Rousseeuw, 1987) provides a graphical representation and an index to measure how well each object lies within its cluster. The silhouette value ( $s$ ) lies between +1 (the object is correctly clustered) and -1 (the object belongs to other cluster).

## 2.4 Urban and regional contributions to the O<sub>3</sub> concentration

To estimate the regional contribution of O<sub>3</sub> to the *in situ* O<sub>3</sub> concentration, we calculated the daylight mean mixing ratios (in ppb) of the oxidant ( $OX = O_3 + NO_2$ ) and NO<sub>x</sub> (Clapp and Jenkin, 2003). The analysis assumes that the interconversion of O<sub>3</sub>, NO<sub>2</sub> and NO occurs in a closed system, where the total mixing ratio of both NO<sub>x</sub> and OX is unchanged. This photostationary state is valid during daylight, hence we considered the hours between 08:00 and 18:00.

Then, a linear regression analysis was performed between OX and NO<sub>x</sub> concentrations, where the offset can be interpreted as NO<sub>x</sub>-independent and the slope as NO<sub>x</sub>-dependent contributions. The former is attributed to regional background O<sub>3</sub> and the latter accounts for the local contribution, which correlates with the level of primary pollution. Any local change in NO<sub>x</sub> concentration will lead to a simultaneous increase or decrease in the concentration of total oxidants (Pancholi *et al.*, 2018; Mazzeo *et al.*, 2005; Clapp and Jenkin, 2003). To investigate this aspect, we chose one city within each cluster with concurrent NO<sub>x</sub>, NO<sub>2</sub> and O<sub>3</sub> measurements.

## 3. Results

### 3.1 Overall O<sub>3</sub> concentrations in different time domains

Figure 1a depicts a statistical summary of O<sub>3</sub> concentrations at all sites between 2014 and 2017. The lowest O<sub>3</sub> concentrations were recorded in June and the highest in September and October. The air quality in South Eastern Brazil is affected by smoke plumes from the Amazon and Cerrado with peak activity in September, caused by the atmospheric transport under the influence of lingering high-pressure systems, which increases air temperatures and enhances photochemistry (Rosário *et al.*, 2013). Another source of air

pollution is the interhemispheric transport of plumes from Africa to Eastern South America, especially in September, October and November, enhancing the tropospheric O<sub>3</sub> column up to 40 Dobson Units (Ziemke *et al.*, 2011).

The stratosphere-troposphere intrusion is a well-documented phenomenon since the early 1960s (Junge, 1962). However, this mechanism is not common in the Southern hemisphere, with the exception for some hotspots observed in June, July and August over the East and West coasts of Australia, and from September to February over the Andes and the southern tip of Africa (Škerlak *et al.*, 2014). Figure 1b suggests a small variation in O<sub>3</sub> amongst the years investigated. However, the Krustal-Wallis test applied at the 5% significance level showed that there are statistically significant differences in O<sub>3</sub> between the years. These differences may be caused by fumigation of upper air masses that is influencing the boundary layer and surface O<sub>3</sub> concentrations, the number of fire outbreaks, regional transport and photochemistry. These mechanisms will not be addressed in this manuscript. The O<sub>3</sub> concentration was consistently higher in the spring months (September and October) for all years investigated in the present study (Fig. 1c).

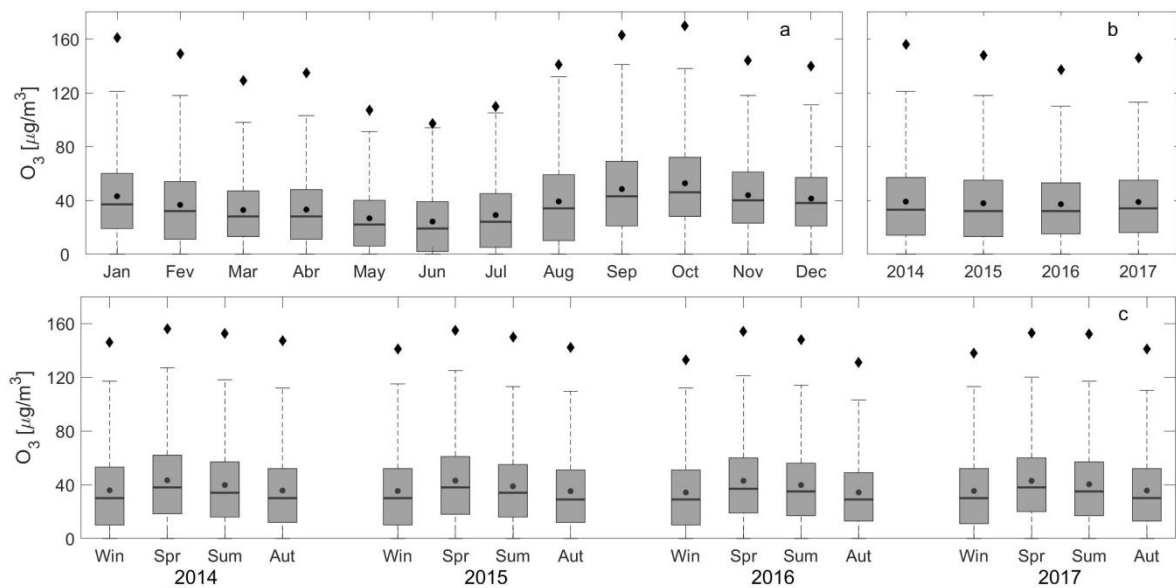


**Figure 1:** Statistical summary of hourly O<sub>3</sub> concentration from 2014 to 2017 for all sites, with respect to a) month, b) year and c) season disaggregated per year. The dots indicate

the mean values, the diamonds are the 99.5 percentile, the whiskers are the 5<sup>th</sup> and 95<sup>th</sup> percentiles, the box limits are the 25<sup>th</sup> and 75<sup>th</sup> percentiles and the black lines across the boxes are median values.

### 3.2 O<sub>3</sub> data reduction based on cluster analysis

The elbow method suggested that the O<sub>3</sub> dataset measured at the 26 sites could be divided into either five or six clusters. However, the silhouette method revealed that choosing six clusters would yield negative *s* values and an overall decrease in the *s* values (between 0.1336 and 0.4660 for five clusters, and between 0 and 0.4324 for six clusters). Another aspect that we also considered to maintain five clusters was the consistency in the location of the stations within each regional area. Figure 2 shows that the stations are distributed across three main areas **Inland:** clusters 1, 2 and 5 (C1, C2 and C5), **Coast:** C3, and **Greater São Paulo and East:** C4.

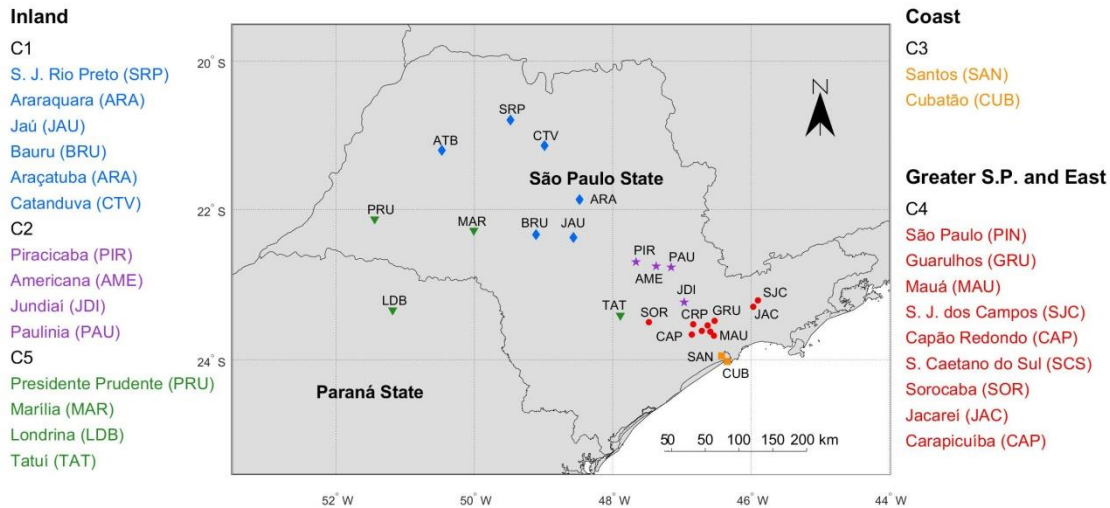


**Figure 2:** Location of the sites investigated in this study. The colours indicate the groups as determined by the cluster analysis and the symbols diamond, star, square, circle and triangle correspond to the groups C1, C2, C3, C4 and C5, respectively.

Figure 3a shows statistic summaries of O<sub>3</sub> for the individual clusters using the datasets from 2014 to 2017, organised in descending order of median values. Overall, the largest O<sub>3</sub> concentrations were recorded at the inland sites and the lowest concentrations at the coastal sites, with mean values varying from 25.2 to 47.6 µg/m<sup>3</sup> and medians from 18.0 to 43.0 µg/m<sup>3</sup>. Even though C2 on average was not the most polluted cluster, the stations in this group had the largest interquartile range and 95<sup>th</sup> percentile. This suggests that the sites within this group were affected by events causing frequently extreme O<sub>3</sub> concentrations. The mean daily O<sub>3</sub> concentrations per cluster (Fig. 3b) showed similar patterns with a large interannual variability along the years investigated. The intercluster correlations using monthly mean O<sub>3</sub> concentrations were statistically significant (*p* values much smaller than 0.05) with Pearson's correlation coefficients (*r*) between 0.75 (C3 and C5) and 0.93 (C2 and C4).

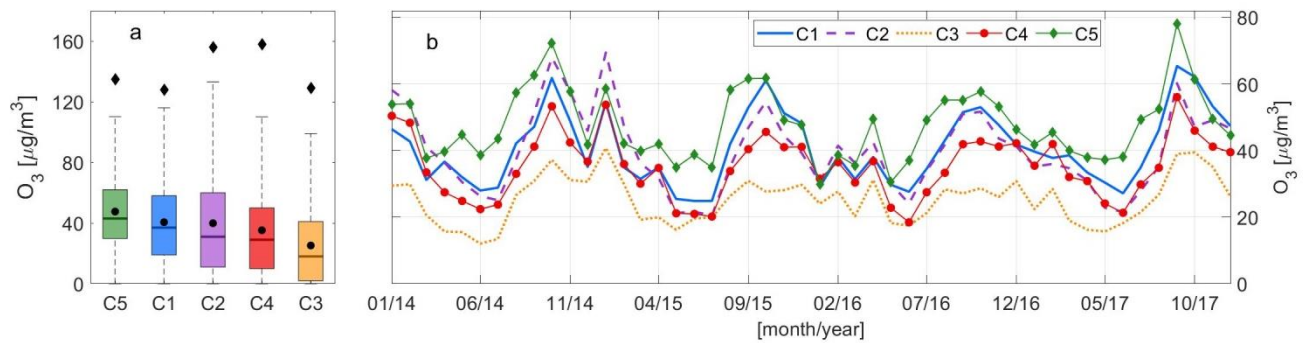


**Figure 3:** (a) Statistical summary of O<sub>3</sub> data for the clustered stations. The dots indicate the mean values, the diamonds are the 99.5<sup>th</sup> percentile, the whiskers are the 5<sup>th</sup> and 9<sup>th</sup> percentiles and the box limits are the 25<sup>th</sup> and 75<sup>th</sup> percentiles and the black lines across the boxes are median values. (b) Mean monthly O<sub>3</sub> concentrations segregated per cluster in the period 2014 – 2017.

### 3.3 Seasonal, weekly and diurnal profiles of O<sub>3</sub> concentrations

Figure 4a shows that the monthly mean  $O_3$  concentration vary seasonally for all clusters, with an increase that begins in July and peaks in September or October. C5 is by far the most polluted cluster from April to September. The comparison between C5 and C3 is particularly striking, with differences in  $O_3$  concentrations of 13.0 and 31.3  $\mu\text{g}/\text{m}^3$  in January and September, respectively. Another outstanding feature is that whilst the  $O_3$  concentrations for C1, C2, C3 and C4 show a clear decrease between January and June, the concentration for C5 remain relatively stable and fluctuate between 36.2 and 43.2  $\mu\text{g}/\text{m}^3$ . Comparatively, the concentration for C4 more than halved over the same period (from 43.1 to 20.8  $\mu\text{g}/\text{m}^3$ ).

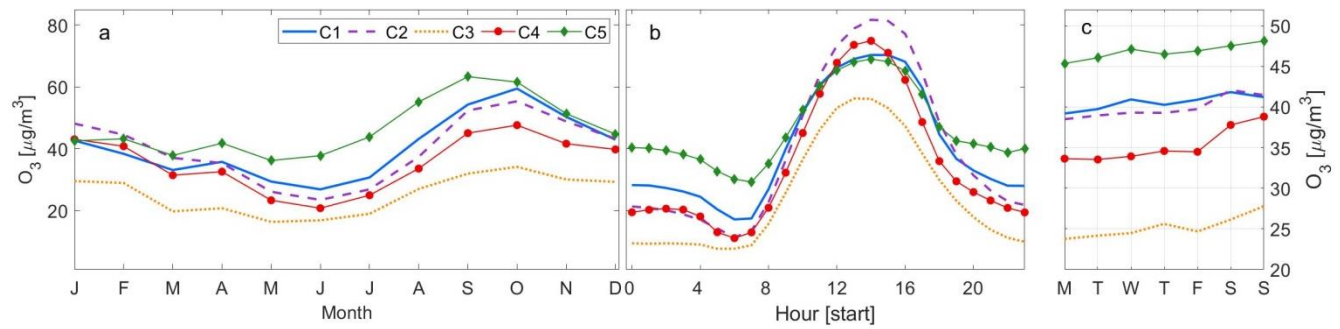


**Figure 4:** (a) Monthly, (b) diurnal and (c) weekly mean  $O_3$  concentrations for the clustered stations.

The clusters show rather similar diurnal patterns, with peak  $O_3$  values in the early afternoon (13:00-15:00, Fig. 4b), with C2 and C4 having the largest peaks and C3 the lowest. C2 and C4 consist mostly of mid-sized and large cities, with traffic volumes that emit large amounts of  $\text{NO}_x$ . However, the reduction of  $\text{NO}$  emissions relative to  $\text{NO}_2$ , typical in urban environments, decreases the  $\text{NO}$  titration effect and increases the daytime  $O_3$  concentration (Querol *et al.*, 2016). This effect was more pronounced for C4, which contains larger cities (including those that form the MASP) and larger vehicle fleets

(Table S1, Supplementary Material). At night, O<sub>3</sub> decreases due to the cease of production, loss mechanisms (dry deposition on the ground) and titration by NO (Monks *et al.*, 2015). C1 and C5 have comparable daytime mean O<sub>3</sub> peak concentration of about 70 µg/m<sup>3</sup>, but diverge at night with concentrations for C5 up to 12 µg/m<sup>3</sup> greater than for C1. C5 has an outstanding secondary nocturnal O<sub>3</sub> peak and the smallest diurnal range. Krecl *et al.* (2016) also observed a secondary O<sub>3</sub> maximum at night in Londrina (a site within C5), which they attributed to horizontal and vertical transport of O<sub>3</sub> from other regions.

The inspection of the diurnal cycle with respect to month showed that this feature prevails along the year and intensifies in September with a maximum nocturnal peak of 55 µg/m<sup>3</sup> (Fig. S1, Supplementary Material). Comparatively, the mean maximum diurnal peak was 92 µg/m<sup>3</sup> at 15:00 in the same month. We hypothesise that two phenomena may control this feature within this group: (i) C5 consists mostly of small cities, Marília (pop. 237,000), Presidente Prudente (pop. 208,000) and (Tatuí, pop. 120,000) (except Londrina, pop. 564,000), that have relatively small traffic volumes to furnish NO and to effectively destroy O<sub>3</sub> at night. Although Londrina's fleet amounts to about 387,000, the sampling site was on the city's outskirts, with little influence from direct vehicular emissions. (ii) Persistent transport of aged pollutants from other regions contributes to a rise in the O<sub>3</sub> nocturnal base line during the year, which is intensified in the spring months due to pollution outbreaks. One pathway is the advection of O<sub>3</sub> from large urban conglomerations, such as MASP. Boian and Andrade (2012) conducted a study using a photochemical model and pinpointed that a nocturnal O<sub>3</sub> peak of 176 µg/m<sup>3</sup> (at 22:00 h) in Campinas (northwest of the city of São Paulo) was due to a plume from the MASP, which still lingered in the early hours. The cities in cluster C5 are all located west of the MASP, and according to INMET (2018) the prevailing wind directions in Presidente



Prudente and Londrina (both within C5) are easterly and easterly/southeasterly, respectively. More precisely, Krecl *et al.* (2016) observed easterly components in Londrina between 00:00 and 10:00 h.

C3 is the cleanest cluster and although Santos and Cubatão have a relatively large fleet (a combined total of 331,600 vehicles) and Cubatão is an industrial city with a cluster of petrochemical, steel and fertilizer industries, they are located on the coast, where frequent overcast weather reduces the incoming solar radiation and inhibits photochemical processes. The mean annual insolation for Santos is 1,376 h with 70% of cloud coverage. For comparison, Londrina in C5 has mean annual insolation of 2,420 h and 50% of cloud coverage (INMET, 2018).

Figure 4c shows that the O<sub>3</sub> concentration tend to increase at weekends, following what has been coined “the ozone weekend effect” (Heuss *et al.*, 2003), attributed to changes in precursors due to the decrease in the traffic volume and travelled distances. Vukovich (2000) and Altshuler *et al.* (1995) showed that the reduction in NO<sub>x</sub> at weekends is more pronounced than for VOC, favouring the O<sub>3</sub> formation due to an increase in the VOC:NO<sub>x</sub> ratio. The weekend effect was more evident for clusters C3 and C4 (Table 1) that consist of highly urbanised areas and have large vehicle fleets. We did not have VOC measurements in this study; however, we refer to the results by Orlando *et al.* (2010) who measured VOC in the MASP and reported a high VOC:NO<sub>x</sub> ratio, especially due to formaldehyde and acetaldehyde. They used model simulations to show that an increase (decrease) in VOCs would result in an increase (decrease) in O<sub>3</sub>. Hence, we suggest that this effect combined with the reduction in O<sub>3</sub> loss due to less titration with NO (Atkinson-Palombo *et al.*, 2006; Torres-Jardon and Keener, 2006; Alghamdi *et al.*, 2014) yields higher O<sub>3</sub> concentrations at weekends within these clusters.

Other pathways for the O<sub>3</sub> weekend effect include: (i) the shift in the timing of NO<sub>x</sub> peak favours O<sub>3</sub> formation at weekends than on weekdays), (ii) carryover of pollutants with higher VOC:NO<sub>x</sub> ratios from light-duty vehicle traffic on Friday and Saturday evenings that can generate more O<sub>3</sub> at weekends, (iii) lower aerosol concentrations at weekends increase incoming solar radiation and photochemistry (Heuss *et al.* (2003).

Table 1: O<sub>3</sub> concentrations in different time domains, derived from hourly mean data.

O <sub>3</sub> [µg/m <sup>3</sup> ]	C1	C2	C3	C4	C5
Diurnal range <sup>a</sup>	53.1	70.3	48.6	63.8	39.7
Diurnal maximum <sup>b</sup>	70.3	81.7	56.3	74.9	69.0
Seasonal range (October - January) <sup>c</sup>	32.6	31.9	17.8	26.8	23.8
Sunday-Monday difference <sup>d</sup>	2.0	3.0	4.0	5.2	2.8

<sup>a</sup>Based on the difference between the mean maximum and minimum diurnal O<sub>3</sub> concentrations.

<sup>b</sup>Maximum O<sub>3</sub> concentration of the diurnal cycle. <sup>c</sup>Based on the difference between the mean monthly O<sub>3</sub> concentrations in October and January. <sup>d</sup>Based on the difference between the mean concentrations for all Sundays and all Mondays.

### 3.4 Pollution outbreak in September 2015

In the austral spring of 2015 an area of about 225,300 km<sup>2</sup> was burned in Brazil, of which 56.0% and 24.5% comprised Cerrado and Amazon biomes, respectively (INPE, 2018). Figure 5 shows MODIS AOD scenes for September 23<sup>rd</sup> 2015 over South America (left) and daily AOD time series along this year (right). It is clearly discernible that enhanced levels of aerosols began to influence the central part of Brazil (right, upper panel) and the state of São Paulo (right, lower panel) in August until the end of the year.

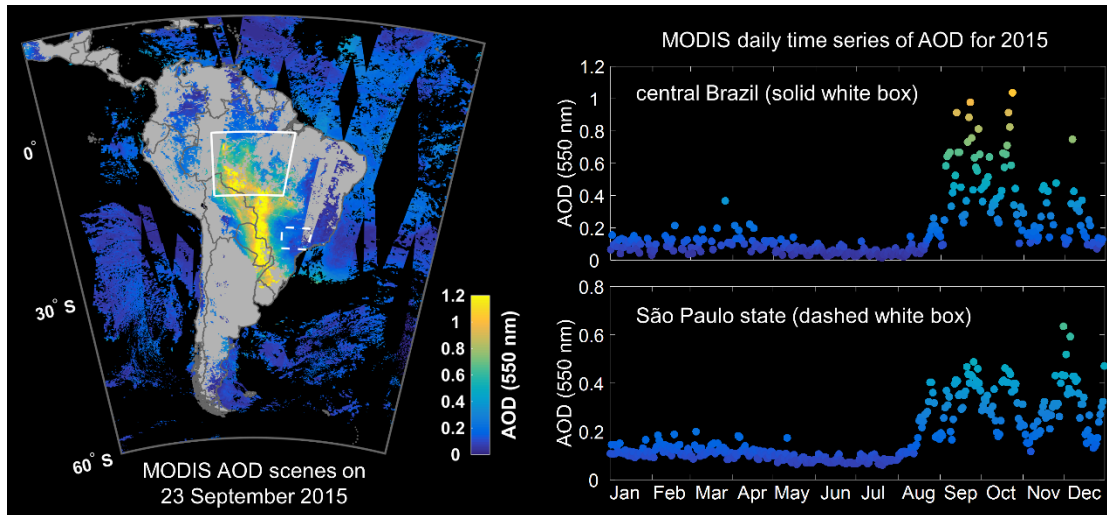


**Fig. 5:** MODIS Aqua and Terra AOD scenes over South America for September 23<sup>rd</sup> 2015 (left), and daily time series of AOD for the central Brazil and the state of São Paulo (right).

We focus here on an air pollution outbreak that led to an enhancement in  $O_3$  concentration and other co-pollutants over the investigated area during the second half of September 2015. Figure 6a shows that the  $O_3$  concentration started to increase around September 15<sup>th</sup> for all clusters, with enhancements between two- and four-fold: for example, from 48.0 to 103.5  $\mu\text{g}/\text{m}^3$  within C3 and from 38.0 to 169.8  $\mu\text{g}/\text{m}^3$  within C4, between September 11<sup>th</sup> and 20<sup>th</sup>. Meteorological data measured at UTFPR campus in Londrina (C5) show that the substantially higher  $O_3$  concentrations that occurred in the afternoon during the period September 14<sup>th</sup>-25<sup>th</sup> coincide with a high-pressure system that led to high temperatures, low relative humidity and strong solar irradiance (for example,  $> 35^\circ\text{C}$ ,  $< 20\%$  and  $> 1,000 \text{ W}/\text{m}^2$ , respectively, in the afternoon of September 23<sup>rd</sup>) (Figures 6b-6d). Such a meteorological situation causes subsiding air to warm adiabatically, inhibits convective mixing and creates a shallow boundary layer where pollutants can accumulate. This is in line with Pudassainee *et al.* (2006) who showed that  $O_3$  production is favoured by increase in air temperature and solar irradiance, and with Querol *et al.*

(2016) who reported very high O<sub>3</sub> concentrations during heat waves in Spain in the summer of 2015.

The surface winds measured at UTFPR campus between September 16<sup>th</sup>-19<sup>th</sup> were northerly and larger than 5.0 m/s in the afternoon, which facilitated advection of polluted air. Between September 20<sup>th</sup>-23<sup>rd</sup> the mean wind speed dropped to 2.7 m/s (Fig. S2, Supplementary Material), reducing the air pollution dispersion and facilitating their accumulation.

Although Figs. 6b-6d illustrate the weather conditions in Londrina, the corresponding meteorological variables correlate well with data from sites within other clusters (see Figs. S3-S8, Supplementary Material). For example, the Pearson's correlation coefficient for hourly air temperature between Londrina and São José do Rio Preto (distance 390 km) and between Londrina and the city of São Paulo (distance 540 km) during the pollution outbreak were 0.95 and 0.91, with linear regression equations of  $1.1x-0.29$  and  $1.0x-2.9$ , respectively, and *p*-values much smaller than 0.05. Only Santos (distance 600 km from Londrina) showed a more modest air temperature increase, yielding weak or moderate correlations with other sites, possibly due to local atmospheric circulations embedded in the large-scale circulation (for example, sea breeze).

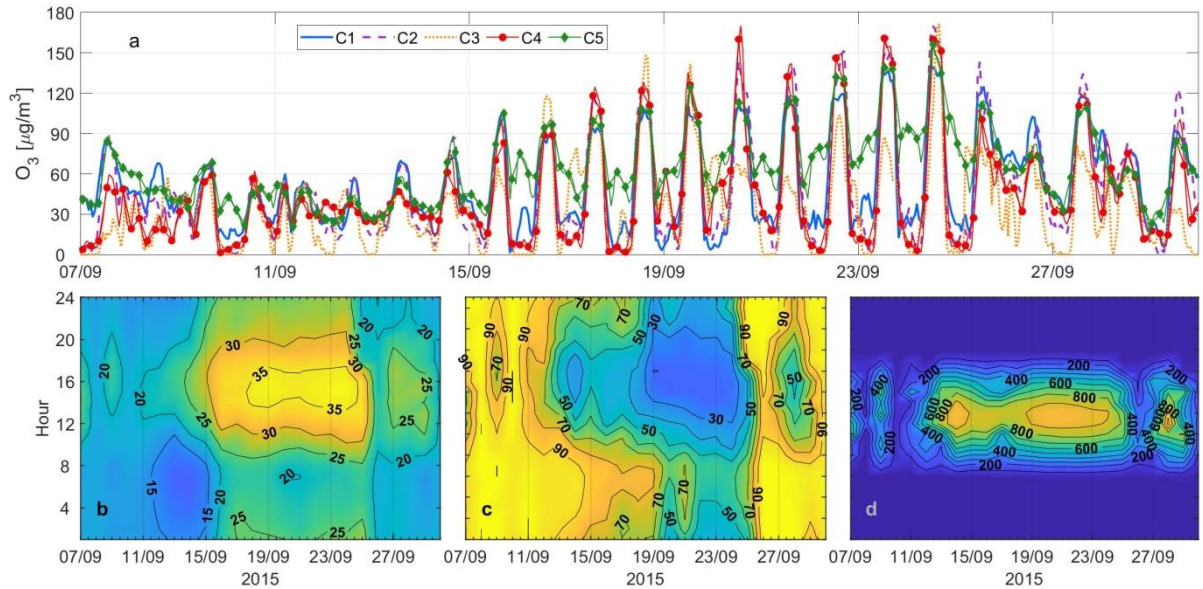


**Fig. 6:** (a) Hourly mean O<sub>3</sub> concentration segregated per cluster, (b) air temperature, (c) relative humidity and (d) solar irradiance measured in Londrina (C5) for the case study in September 2015.

Figure 7 suggests that air masses that arrived at 500 m above ground level in Londrina in the period September 9<sup>th</sup>-13<sup>th</sup> (prior to the pollution event) had either maritime origin or mainly passed over land areas unaffected by fire spots (red dots).

Areas closer to the receptor point were highly influenced by fires from September 15<sup>th</sup> (Fig. 7). Four days prior to and during the pollution events (September 7<sup>th</sup>-14<sup>th</sup> and September 15<sup>th</sup>-24<sup>th</sup>, respectively), the mean AOD and corresponding one standard deviation for the state of São Paulo (20-24°S, 45-52°W) were  $0.23 \pm 0.07$  and  $0.39 \pm 0.06$ , respectively. Satellite data provided by INPE indicated an increase of 42% in the occurrence of fire spots in Brazil in the episode period compared to the non-episode period. Particularly, the numbers of fire spots in the states of Paraná and São Paulo increased from 316 to 2,719 and from 68 to 2,302 spots, respectively (Figs. S9 and S10). Table 2 displays statistics of O<sub>3</sub> concentration within each clusters before and during the pollution event.

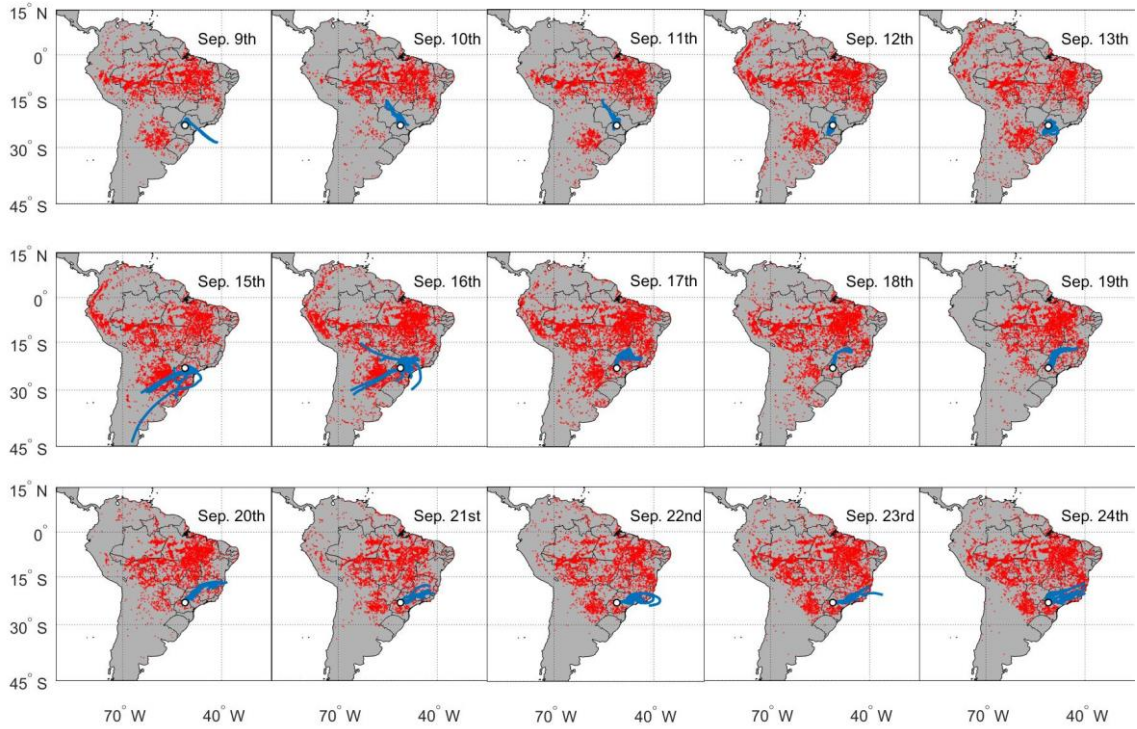


**Fig. 7:** Fire spots (red dots) over South America and five-day backward trajectories (blue solid lines) before (first row) and during the pollution outbreak (second and third rows).  
 Table 2: Comparison of mean hourly ( $\pm$  one standard deviation) and maximum  $O_3$  concentrations before and during the pollution outbreak in September 2015.

$O_3$	C1	C2	C3	C4	C5
$[\mu g/m^3]$	Before the pollution outbreak				
Mean	$40.4 \pm 17.0$	$34.1 \pm 20.6$	$24.4 \pm 17.6$	$30.0 \pm 15.1$	$43.9 \pm 14.4$
Maximum	85.8	87.2	58.0	74.0	88.6
	During the pollution outbreak				
Mean	$54.4 \pm 40.4$	$54.2 \pm 49.0$	$43.4 \pm 38.2$	$52.4 \pm 49.0$	$79.8 \pm 28.5$
Maximum	140.3	169.8	171.5	170.0	156.2

The pollution outbreak was captured across the state of São Paulo, as shown by the evolution of O<sub>3</sub>, NO<sub>x</sub>, PM<sub>2.5</sub> and PM<sub>10</sub> at sites representative of each cluster (Fig. 8 and Table 3): São José do Rio Preto (C1), Piracicaba (C2), Santos (C3), São Paulo (C4) and Marília (C5). During this event, a large increase in nocturnal O<sub>3</sub> concentration was observed in Marília and Santos. The results on diurnal cycles (Section 3.3) had already revealed that C5 presented a secondary nocturnal O<sub>3</sub> peak. However, the peak recorded in Marília during this pollution outbreak ( $> 100 \mu\text{g m}^{-3}$  on September 23<sup>rd</sup>) was much larger than observed even in the dirtiest month (Fig. S1, Supplementary Material). The nocturnal peak observed in Santos ( $> 60 \mu\text{g m}^{-3}$ ) was an uncommon feature compared to the diurnal cycle for C4. The enhancement of NO<sub>x</sub> was observed at all sites, especially at night, due to the increase in NO<sub>2</sub> via NO-to-O<sub>3</sub> conversion, with mean episode:non-episode NO<sub>x</sub> ratios ranging from 1.4 (Santos) to 3.5 (São José do Rio Preto). The particulate concentrations showed a very sharp increase starting on September 15<sup>th</sup>, with higher concentrations occurring generally in the early morning and late evening hours. The diurnal variation was due to the increase in the boundary layer height in the afternoon –which favours dilution of the pollutants– and by a shallow layer in the evening, as shown by three-hour resolution ERA-Interim reanalysis data taken from the ECMWF (Fig. S11). Pollutant concentrations greatly exceeded the thresholds recommended by the World Health Organisation (WHO), whereas in a few occasions were the Brazilian air quality standards for PM<sub>2.5</sub> and PM<sub>10</sub> (60 and 120  $\mu\text{g/m}^3$ , respectively) exceeded. This occurred only once at Pinheiros in Greater São Paulo and Piracicaba on September 24<sup>th</sup> (65.5 and 134.2  $\mu\text{g/m}^3$ , and 62 and 141  $\mu\text{g/m}^3$ , respectively). However, all clusters exceeded the daily WHO limits for PM<sub>2.5</sub> or PM<sub>10</sub> (25 and 50  $\mu\text{g/m}^3$ , respectively) at least five out of 10 days of the duration of the event (São José do Rio Preto exceeded the PM<sub>10</sub> limit on 10 days). Santos, on the other hand, surpassed the PM<sub>10</sub> limit only once (53  $\mu\text{g/m}^3$  on

September 24<sup>th</sup>). McClure and Jaffe (2018b) found that wildfires caused a significant increase in the 98<sup>th</sup> quartile PM<sub>2.5</sub> concentrations at sites in the northwest United States (average  $0.21 \pm 0.12 \text{ } \mu\text{g}/\text{m}^3/\text{year}$ ), and Targino *et al.* (2013) reported that the concentration of accumulation-mode particles increased by 40 and 340% at urban and rural sites, respectively, in Sweden due to the outflow of wildfire plumes from Eastern Europe.

The Brazilian standard for O<sub>3</sub> (maximum daily 8-hour moving mean of  $140 \text{ } \mu\text{g}/\text{m}^3$ ) was exceeded only in Marília (three days), Piracicaba (four days) and São Paulo (one day). However, when considering the WHO guideline of  $100 \text{ } \mu\text{g}/\text{m}^3$ , Marília exceeded the limits on all days investigated here, Piracicaba on eight days, São Paulo on four days and São José do Rio Preto on three days. As the increase in O<sub>3</sub> was accompanied by substantial increase in both PM<sub>2.5</sub> and PM<sub>10</sub>, it is evident that the long-rang transport of smoke severely deteriorates the air quality in cities of all sizes, and can outweigh measures to curb local air pollution.

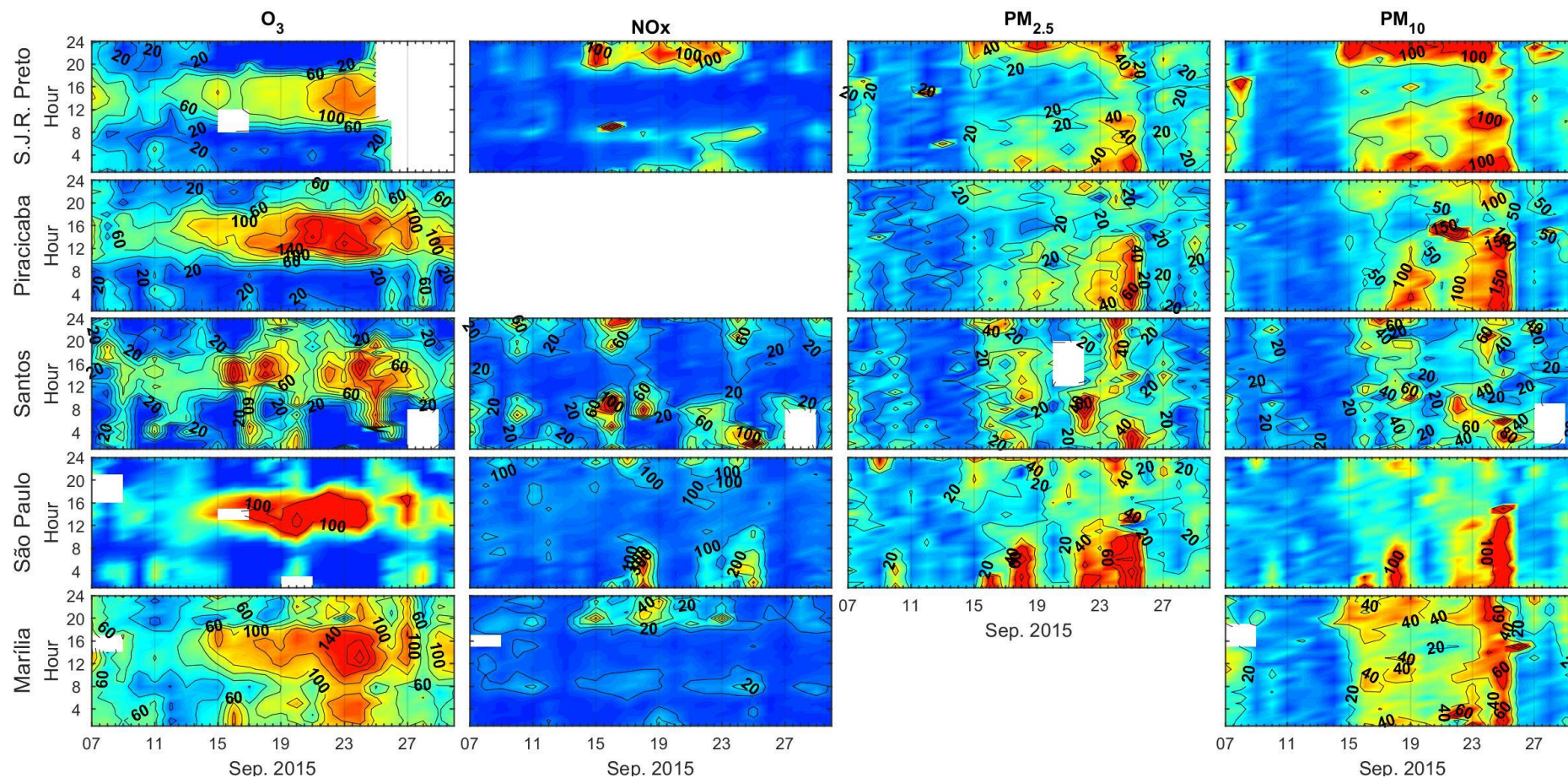


Cluster	Site	O <sub>3</sub>			NO <sub>x</sub>			PM <sub>2.5</sub>			PM <sub>10</sub>		
		(µg/m <sup>3</sup> )											
		Mean	P5	P95	Mean	P5	P95	Mean	P5	P95	Mean	P5	P95
C1	São J. Rio Preto												
	Non-episode	41.2	11.1	79.9	11.1	3.0	27.9	12.3	1.1	30.0	22.9	6.1	58.8
	Pollution outbreak	<sup>a</sup> 41.5	<sup>a</sup> 1.0	<sup>a</sup> 118.9	38.9	4.0	125.0	27.0	9.0	50.5	65.8	29.5	118.5
C2	Piracicaba												
	Non-episode	41.7	4.1	89.0	n.m.	n.m.	n.m.	11.8	3.0	25.0	24.8	9.0	57.8
	Pollution outbreak	61.1	3.0	157.5				25.3	10.0	43.0	78.2	30.0	138.5
C3	Santos												
	Non-episode	24.3	1.0	54.8	24.4	4.0	64.9	11.4	1.0	27.0	15.8	3.0	36.0
	Pollution outbreak	39.0	1.0	91.0	34.7	4.0	110.0	25.3	4.0	51.8	36.4	10.0	74.0
C4	S. Paulo (Pinheiros)												
	Non-episode	23.3	0.9	50.0	41.2	12.6	86.9	11.1	1.0	26.2	16.4	1.0	44.6
	Pollution outbreak	39.7	1.0	131.0	103.2	12.1	284.6	25.3	1.5	66.2	49.0	9.0	84.1
C5	Marília												
	Non-episode	52.7	23.0	83.0	7.2	2.0	17.0	n.m.	n.m.	n.m.	14.7	4.0	37.1
	Pollution outbreak	96.8	41.0	150.0	12.4	3.0	37.5				36.6	19.0	53.0

493 Table 3: Summary of pollutant concentrations during the non-episode (September 7<sup>th</sup>-14<sup>th</sup>) and pollution outbreak (and September 15<sup>th</sup>-24<sup>th</sup>) periods  
494 for sites representative of each cluster.

495

496 <sup>a</sup>This value may not be representative due to reduced number of observations. n.m. Not measured at this site.



497

498 **Fig. 8:** Hourly  $O_3$ ,  $NO_x$ ,  $PM_{2.5}$  and  $PM_{10}$  concentrations measured in September 2015 at selected sites in the state of São Paulo.

### 3.5 OX analysis and estimates of local and long-range contribution

To disentangle the local and regional contributions of O<sub>3</sub> across the study area, we picked the cities discussed in the previous section due to the availability in NO<sub>x</sub>, NO<sub>2</sub> and O<sub>3</sub> measurements. Besides analysing the NO<sub>x</sub>-OX relationship for all sites and months we split the data into three-month periods, since we observed that August, September and October were the most polluted months (Fig. 4a). We grouped the months as follows: (i) February, March and April, (ii) May, June and July, (iii) August, September and October, and (iv) November, December and January.

Figure 9a shows the NO<sub>x</sub>-OX relationship for all sites irrespective of the time of the year, and Figs 9b-f subdivided with respect to site and season. Also shown are the linear regression equations and Pearson's correlation coefficient (for all cases, the *p*-values were much smaller than 0.05). We found a positive linear increase of OX with NO<sub>x</sub>, with a mean intercept of 31 ppb (60.8 µg/m<sup>3</sup>), which can be interpreted as the regional O<sub>3</sub> contribution. This is in line with previous studies by Pancholi *et al.* (2018), Mazzeo *et al.* (2005) and Clapp and Jenkin (2003) who reported regional contributions of 59, 43 and 70 µg/m<sup>3</sup> for Jodhpur (India), Buenos Aires (Argentina) and London (UK), respectively. However, when inspecting our results with respect to site and season we found different strengths of the regional contribution (Figs. 9b-f). The largest regional O<sub>3</sub> contribution at all sites was found for the biomass burning season (August-October). Clapp and Jenkin (2001) also found that the regional contribution increased from 76 µg/m<sup>3</sup> on non-episode days to 109 µg/m<sup>3</sup> on episode days in London (the latter was defined as days in April-September affected by regional-scale photochemical events). We found that during the polluted season in South Eastern Brazil, small cities received a relatively large regional contribution. For example, the mean annual O<sub>3</sub> concentration ( $\pm$  one standard deviation) in Marília was only 26.1 $\pm$ 12.6 ppb (51.2 $\pm$ 24.6 µg/m<sup>3</sup>). However, the regional transport

may account for as much as 41.4% of the total O<sub>3</sub> in Marília when considering the maximum concentration observed during the biomass burning season (99 ppb). The regional contribution of O<sub>3</sub> for Piracicaba, Santos, São Paulo and São José do Rio Preto, considering the most extreme O<sub>3</sub> concentrations in the same period (117.4, 65.8, 151.5 and 98 ppb, respectively) were 36.6, 38.0, 23.1 and 37.8%.

We found a large variability in local OX with respect to season, and the largest contribution was observed in summer at all sites (November-January). This term is contributed by primary NO<sub>2</sub> emissions, typically 5-15% of NO<sub>x</sub>, and local O<sub>3</sub> formation, which depends on the sources of NO<sub>x</sub>. In urban areas, on-road transport are the dominating sources and NO<sub>2</sub> enters the atmosphere mostly via the reaction:



Hence, in most cases the local production will depend on the fleet characteristics, fuel composition and traffic volumes (Carslaw, 2005). However, a source apportionment study for the mega city of São Paulo showed a slightly different scenario in which not only exhaust from on-road transport, but also industrial activities and biomass burning (both local and remote) contributed to the air pollution in the city (Pereira *et al.*, 2017), and, thus, can be sources of NO<sub>x</sub>.

We found a large variability in local OX with respect to season, and the largest contribution was observed in summer at all sites (November-January). The smallest slopes were observed in São Paulo and Santos (< 1), regardless of the period of the year (see equations in Fig. 9 and S12 for a month-by-month variability). Clapp and Jenkin (2003) and Notario *et al.* (2012) showed that the local contribution at sites in the UK and

Spain also peaked in summer, which has been attributed to higher solar irradiance and enhanced photochemistry.

We calculated the NO<sub>2</sub>:OX ratios from hourly data and a positive trend was identified with increasing NO<sub>x</sub> concentration (Fig. S13 Supplementary Material). According to the mean NO<sub>2</sub>:OX ratios, the selected sites can be classified within two groups: one with mean ratios higher than 0.35 (São Paulo and Santos) and the second group with ratios substantially lower (São José do Rio Preto, Marília and Piracicaba) (Table 4).

Cluster	Site	Feb-Mar-Apr	May-Jun-Jul	Aug-Sep-Oct	Nov-Dec-Jan
C2	Piracicaba	0.17±0.09	0.31±0.17	0.18±0.08	0.12±0.06
C4	São Paulo	0.49±0.19	0.67±0.18	0.51±0.17	0.40±0.17
C1	São José Rio Preto	0.20±0.08	0.28±0.12	0.21±0.13	0.21±0.19
C3	Santos	0.41±0.15	0.51±0.22	0.36±0.14	0.35±0.14
C5	Marília	0.16±0.06	0.23±0.09	0.14±0.06	0.14±0.08

Table 4: Summary of mean (± standard deviation) NO<sub>2</sub>:OX ratios segregated by site and season in the period 2014-2017.

The differences in the partitioning can be partially attributed to:

(i) Photochemical processes. The lower insolation in Santos and, to a lesser degree in São Paulo (1,895 h/year) makes the reaction



less efficient than at the other sites, since the rate of NO<sub>2</sub> photolysis is a function of solar radiation intensity (actinic flux), which can be attenuated by cloud scattering. This effect

preserves NO<sub>2</sub> and increases the NO<sub>2</sub>:OX ratio, especially in winter (May, June and July) (Table 4).

(ii) Proximity to exhaust emissions from diesel light-duty vehicles. Grange *et al.* (2017) showed a clear positive trend in NO<sub>2</sub> directly emitted by diesel passenger cars in Europe in the period 1995-2010, reaching about 15% of the total NO<sub>x</sub> in 2010. Although, current Brazilian regulations prohibit the sales of diesel passenger cars, light-duty vehicles for commercial purposes and sport utility vehicles (SUV) run on diesel and largely penetrated the Brazilian market since 2008. Nowadays, 46% of the sales of light-duty vehicles correspond to diesel-fuelled units and represent 6.8% of the total market sales (ANFAVEA, 2019). These vehicles have emission standards mostly equivalent to Euro 3, 4 and 5.

Despite the lack of studies on trends in the NO<sub>2</sub>:NO<sub>x</sub> ratio for Brazil, we hypothesise that direct NO<sub>2</sub> emissions from diesel vehicles increased in recent years. This effect may have been captured by the measurements at São Paulo Pinheiros site, which is located on the kerb of Frederico Hermann street –a eight-lane road used for traffic and kerbside parking. Moreover, the site is only 230 m from the highly trafficked Marginal Pinheiros ring road, where congestion frequently occurs and the proportion of diesel-fuelled vehicles is high.



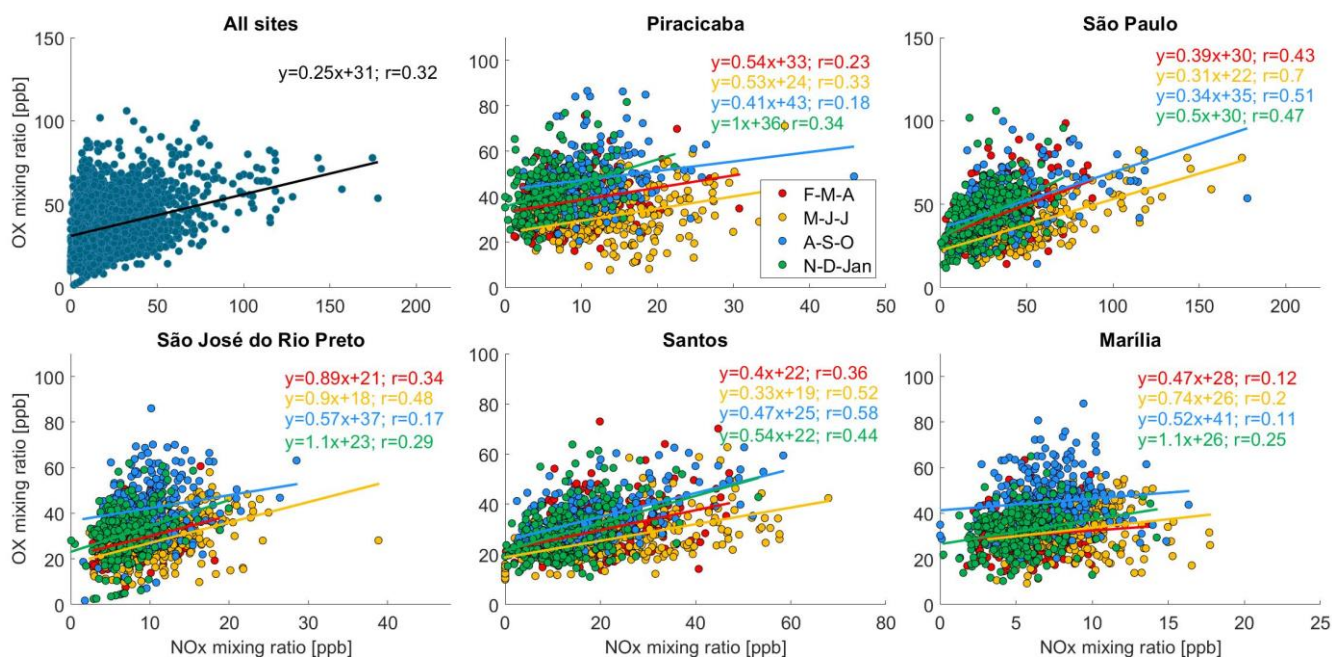


**Fig. 9:** Variation in mean daylight mixing ratios of OX with respect to NOx. The lines were obtained by linear regression analysis. Also shown are linear regression equations and the Pearson's correlation coefficient.

#### 4. Summary and conclusions

Applying a hierarchical clustering technique on hourly O<sub>3</sub> data collected in the period 2014-2017 at 26 sites in the states of São Paulo and Paraná, Brazil, enabled us to reduce the dataset to five homogenous groups with respect to seasonal, monthly, weekly and diurnal concentrations. The cleanest group was located on the coast whilst the inland sites showed the highest concentrations. Group C5 (inland) stood out with a pronounced mean annual nocturnal O<sub>3</sub> peak of 40 µg/m<sup>3</sup>, which reached 55 µg/m<sup>3</sup> in September. Comparatively, the mean annual diurnal peak was 63 µg/m<sup>3</sup>. We attributed this peak to the combined effects of transported smoke from biomass burning and sustained outflow of aged pollution from the metropolitan area of São Paulo. All groups were associated with peak O<sub>3</sub> concentrations in September or October, with mean values between 34 and 63 µg/m<sup>3</sup>, coinciding with the biomass burning season in central and northern Brazil. The

overall mean regional O<sub>3</sub> contribution during the polluted period was 61 µg/m<sup>3</sup>, with a great seasonal and intersite variability, ranging from 35 to 84 µg/m<sup>3</sup>. We found that the long-range transport of smoke can contribute with between 23 and 41 % of the total O<sub>3</sub>. Investigation of a pollution outbreak in September 2015 showed that the smoke caused sharp increases in O<sub>3</sub>, PM<sub>2.5</sub> and PM<sub>10</sub> concentrations and exceedances in the levels recommended by the WHO. All cities were affected with between 2.2- and 3.1-fold increases in PM<sub>10</sub>, 2-fold increase in PM<sub>2.5</sub>, between 1.5- and 1.8-fold increases in O<sub>3</sub> and between 1.4- and 3.5-fold increases in NO<sub>x</sub> concentrations compared to the non-episode period. This indicates that biomass burning, both in remote and proximate areas, increases gas and particulate concentrations and quickly deteriorates the air quality of small and big cities. Depending on the large-scale circulation, the exceedances in air quality standards can last for several days and outweigh the reductions in anthropogenic sources that are promoted to curb air pollution in cities (for example, on-road traffic exhaust emissions). Analysis of the local oxidant sources showed a substantial variability across the study area and a seasonal dependence. More specifically, larger contributions in the period November-January due to enhanced photochemistry. The local oxidant contribution was lower in the cities of São Paulo and Santos, compared to the inland sites.

The state of São Paulo has always been at the forefront in terms of progressive measures to curb air pollution, by introducing programs to control sulphur dioxide from industrial sources and by enforcing standards for cleaner vehicles and fuels. However, the present results indicate that policies targeting the reduction of biomass burning is of outmost importance to improve the urban air quality, particularly in densely populated areas where high pollutant concentrations are frequently observed. This can only be achieved with enhanced governance acting at regional, national and international levels to combat biomass burning practices in Brazil and its neighbouring countries. Not only the



population health would benefit from such a measure, but also the regional climate, since O<sub>3</sub>, BC and PM<sub>2.5</sub> are short-lived climate forcers (SLCF).

This strategy would be well-aligned with the Paris Agreement that aims to limit global warming to below 2 °C compared to pre-industrial, and which must be complemented with the reduction of SLCF emissions.

## Acknowledgments

The authors thank CETESB, ECMWF and INPE for providing data for this study and Prof. Jorge Alberto Martins for furnishing the weather data collected at the campus of the Federal University of Technology.

**Declaration of interest:** None

## References

- Akagi, S.K., Yokelson, R.J., Wiedinmyer, C., Alvarado, M.J., Reid, J.S., Karl, T., Crounse, J. D., and Wennberg, P.O., 2011. Emission factors for open and domestic biomass burning for use in atmospheric models. *Atmos. Chem. Phys.*, 11, 4039–4072.
- ANFAVEA, 2019. Brazilian automotive industry yearbook 2019 (<http://www.anfavea.com.br/anuarios.html>). Last accessed 24 April 2019.
- Alghamdi, M.A., Khoder, M., Harrison, R.M., Hyvärinen, A.-P., Hussein, T., Al-Jeelani, H., Abdelmaksoud, A.S., Goknil, M.H., Shabbaj, I.I., Almehmadi, F.M., Lihavainen, H., Kulmala, M., and Hameri, K. 2014. Temporal variations of O<sub>3</sub> and NO<sub>x</sub> in the urban background atmosphere of the coastal city Jeddah, Saudi Arabia. *Atmos. Environ.*, 94, 205-214.

653 Allen, A.G., Cardoso, A.A., Rocha, G.O., 2004. Influence of sugar cane burning on  
654 aerosol soluble ion composition in Southeastern Brazil. *Atmos. Environ.*, 38, 5025–  
655 5038.

656 Altshuler, S.L., Arcado, T.D., Lawson, D.R., 1995. Weekday vs. weekend ambient ozone  
657 concentrations: Discussion and hypotheses with focus on northern California. *J. Air*  
658 *Waste Manage. Assoc.*, 45, 967-972.

659 Alvarado, M., Lonsdale, C., Yokelson, R., Akagi, S.K., Coe, H., Craven, J., Fischer, E.,  
660 McMeeking, G., Seinfeld, J., Soni, T., 2015. Investigating the links between ozone and  
661 organic aerosol chemistry in a biomass burning plume from a prescribed fire in  
662 California chaparral. *Atmos. Chem. Phys.*, 15, 6667–6688.

663 Atkinson-Palombo, C.M., Miller, J.A., and Balling, R.C. Jr., 2006. Quantifying the ozone  
664 “weekend effect” at various locations in Phoenix, Arizona. *Atmos. Environ.*, 40, 7644-  
665 7658.

666 Baylon, P., Jaffe, D., Hall, S., Ullmann, K., Alvarado, M., Lefer, B., 2018. Impact of  
667 biomass burning plumes on photolysis rates and ozone formation at the Mount  
668 Bachelor observatory. *J. Geophys. Res.*, 123, 2272–2284.

669 Boian, C., Andrade, M.F., 2012. Characterization of ozone transport among metropolitan  
670 regions. *Rev. Bras. Meteorol.*, 27, 229-242.

671 Carslaw, D.C., 2005. Evidence of an increasing NO<sub>2</sub>/NO<sub>x</sub> emissions ratio from road  
672 traffic emissions. *Atmos. Environ.*, 39, 4793-4802.

673 Clapp, L.J., Jenkin, M.E., 2003. Analysis of the relationship between ambient levels of  
674 O<sub>3</sub>, NO<sub>2</sub> and NO as a function of NO<sub>x</sub> in the UK. *Atmos. Environ.*, 35, 6391-6405.

675 Crippa, M., Guizzardi, D., Muntean, M., Schaaf, E., Dentener, F., van Aardenne, J.A.,  
676 Monni, S., Doering, U., Olivier, J.G.J., Pagliari, V. and Janssens-Maenhout, G., 2018.  
677 Gridded Emissions of Air Pollutants for the period 1970–2012 within EDGAR v4.3.2  
678 *Earth Syst. Sci. Data*. <https://doi.org/10.5194/essd-10-1987-2018>.

679 Crutzen, P.J., Andreae, M.O., 1990. Biomass burning in the tropics: Impact on  
680 atmospheric chemistry and biogeochemical cycles. *Science*, 250, 1669–1678.

681 Flannigan, M. D., Krawchuk, M. A., de Groot, W. J., Wotton, B. M., Gowman, L. M.,  
682 2009. Implications of changing climate for global wildland fire. *Int. J. Wildland Fire*,  
683 18, 483–507.

684 Flannigan, M., Cantin, A.S., de Groot, W.J., Wotton, M., Newbery, A., Gowman, L.M.,  
685 2013. Global wildland fire season severity in the 21st century. *For. Ecol. Manag.*, 294,  
686 54–61.

687 Freitas, S.R., Longo, K.M., Dias, M.A.F.S., Dias, P.L.S., Chatfield, R., Prins, E., Artaxo,  
688 P., Grell, G.A., Recuero, F.S., 2005. Monitoring the transport of biomass burning  
689 emissions in South America. *Environ. Fluid Mech.*, 5, 135–167.

690 Gandhi, O., Oshiro, A.H., Costa, H.K.M., Santos, E.M., 2017. Energy intensity trend  
691 explained for Sao Paulo state. *Renew. Sust. Energ. Rev.*, 77, 1046-1054.

692 Governo do Estado de São Paulo, 2019. (<http://www.saopauloglobal.sp.gov.br/>) (Last  
693 accessed 12 February 2019).

694 Grange, S.K., Lewis, A.C., Moller, S.J., Carslaw, D.C., 2017. Lower vehicular primary  
695 emissions of NO<sub>2</sub> in Europe than assumed in policy projections. *Nat. Geosci.*, 10, 914-  
696 918.

697 Hair, J. F , Tatham, R. L., Anderson, R. E., Black, W., 1998. Multivariate Data Analysis.  
698 5th ed. Prentice Hall International, London.

699 Heuss, J.M., Kahlbaum, D.F., Wolff, G.T., 2003. Weekday/Weekend ozone differences:  
700 What can we learn from them? *J. Air Waste Manage. Assoc.*, 53, 772-788.

701 INPE, 2018. National Institute for Space Research. Portal for the monitoring of vegetation  
702 fires. Available at <http://www.inpe.br/queimadas>. Last accessed October 21, 2018.

703 INMET, 2018. Instituto Nacional de Meteorologia. Normais Climatológicas do Brasil  
704 1981-2010. Available at <http://www.inmet.gov.br>. Last accessed on April 04, 2019.

705 Jenkin, M.E., Clemitshaw, K.C., 2000. Ozone and other secondary photochemical  
706 pollutants: chemical processes governing their formation in the planetary boundary  
707 layer. *Atmos. Environ.*, 34, 2499–2527.

708 Jerrett, M., Burnett, R.T., Pope, C.A., Ito, K., Thurston, G., Krewski, D., Shi, Y.L., Calle,  
709 E., Thun, M., 2009. Long-term ozone exposure and mortality. *N. Engl. J. Med.*, 360,  
710 1085-1095.

711 Junge, C.E., 1962. Global ozone budget and exchange between stratosphere and  
712 troposphere. *Tellus*, 4, 363-377.

713 Kalkstein, L. S., Corrigan, P., 1986. A synoptic climatological approach for geographical  
714 analysis: Assessment of sulfur dioxide concentrations. *Ann. Assoc. Amer. Geo.*, 76,  
715 381-395.

716 Krawchuk, M.A., Moritz, M.A., Parisien, M.-A., Van Dorn, J., Hayhoe, K., 2009: Global  
717 pyrogeography: the current and future distribution of wildfire. *PLoS ONE*, 4(4),  
718 DOI:10.1371/journal.pone.0005102.

719 Krecl, P., Targino, A.C., Wiese, L., Ketzel, M., 2016. Screening of short-lived climate  
720 pollutants in a street canyon in a mid-sized city in Brazil. *Atmos. Poll. Res.*, 7, 1022-  
721 1036.

- Levy, R.C., Remer, L.A., Mattoo, S., Vermote, E.F., Kaufman, Y. J., 2007. Second-generation operational algorithm: Retrieval of aerosol properties over land from inversion of Moderate Resolution Imaging Spectroradiometer spectral reflectance. *J. Geophys. Res. Atmos.*, 112, D13211, doi:10.1029/2006JD007811.
- Levy, R.C., Mattoo, S., Munchak, L.A., Remer, L.A., Sayer A.M. and co-authors, 2013. The Collection 6 MODIS aerosol products over land and ocean. *Atmos. Meas. Tech.*, 6, 2989-3034.
- Lin, Y. C., Lin, C. Y., Lin, P. H., Engling, G., Lin, Y. C., Lan, Y. Y., Chang, C. W. J., Kuo, T. H., Hsu, W. T., Ting, C. C., 2013. Influence of Southeast Asian biomass burning on ozone and carbon monoxide over subtropical Taiwan, *Atmos. Environ.*, 64, 358-365.
- Lopes, F.J.S., Mariano, G.L., Landulfo, E., Mariano, E.V.C., 2012. Impacts of biomass burning in the atmosphere of the southeastern region of Brazil using remote sensing systems. *Atmospheric Aerosols*, IntechOpen, DOI: 10.5772/50406.
- Lyapina, O., Schultz, M.G., Hense, A., 2016. Cluster analysis of European surface ozone observations for evaluation of MACC reanalysis data. *Atmos. Chem. Phys.*, 16, 6863–6881.
- Mazzeo, N.A., Venegas, L.E., Choren, H., 2005. Analysis of NO, NO<sub>2</sub>, O<sub>3</sub> and NO<sub>x</sub> concentrations measured at a green area of Buenos Aires City during wintertime. *Atmos. Environ.*, 39, 3055–3068.
- McClure, C.D., Jaffe, D.A., 2018a. Investigation of high ozone events due to wildfire smoke in an urban area. *Atmos. Environ.*, 194, 146-157.
- McClure, C.D., Jaffe, D.A., 2018b. US particulate matter air quality improves except in wildfire-prone areas. *PNAS*, 115, 7901–7906.

746 Monks, P.S., Archibald, A.T., Colette, A., Cooper, O., Coyle, M., Derwent, R., Fowler,  
 747 D., Granier, C., Law, K. S., Mills, G. E., Stevenson, D.S., Tarasova, O., Thouret, V.,  
 748 von Schneidemesser, E., Sommariva, R., Wild, O., and Williams, M.L., 2015.  
 749 Tropospheric ozone and its precursors from the urban to the global scale from air  
 750 quality to short-lived climate forcer. *Atmos. Chem. Phys.*, 15, 8889–8973.

751 Notario, A., Bravo, I., Adame, J.A., Díaz-de-Mera, Y., Aranda, A., Rodríguez, A.,  
 752 Rodríguez, D., 2012. Analysis of NO, NO<sub>2</sub>, NO<sub>x</sub>, O<sub>3</sub> and oxidant (OX=O<sub>3</sub>+NO<sub>2</sub>)  
 753 levels measured in a metropolitan area in the southwest of Iberian Peninsula. *Atmos.*  
 754 *Res.*, 104, 217–226.

755 Oliveira, A.M., Mariano, G.L., Alonso, M.F., Mariano, E.V.C., 2016. Analysis of  
 756 incoming biomass burning aerosol plumes over southern Brazil. *Atmos. Sci. Let.*, DOI:  
 757 doi.org/10.1002/asl.689.

758 Pancholi, P., Kumar, A., Bikundia, D.S., Chourasiya, S., 2018. An observation of  
 759 seasonal and diurnal behavior of O<sub>3</sub>-NO<sub>x</sub> relationships and local/regional oxidant (OX  
 760 = O<sub>3</sub> + NO<sub>2</sub>) levels at a semi-arid urban site of western India. *Sust. Environ. Res.*, 28,  
 761 79-89.

762 Pereira, G.M., Teinilä, K., Custódio, D., Santos, A.G., Xian, H., Hillamo, R., Alves, C.  
 763 A., Andrade, J.B., Rocha, G.O., Kumar, P., Balasubramanian, R., Andrade, M.F.,  
 764 Vasconcellos, P.C., 2017. Particulate pollutants in the Brazilian city of São Paulo: 1-  
 765 year investigation for the chemical composition and source apportionment. *Atmos.*  
 766 *Chem. Phys.*, 17, 11943-11969.

767 Pivello, V.R., 2011. The use of fire in the Cerrado and Amazon rainforests of Brazil: Past  
 768 and present. *Fire Ecol.*, 7, 24-39.

769 Pudasainee, D., Sapkota, B., Shrestha, M.L., Kaga, A., Kondo, A., Inoue, Y., 2006:  
 770 Ground level ozone concentrations and its association with NO<sub>x</sub> and meteorological  
 771 parameters in Kathmandu valley, Nepal. *Atmos. Environ.*, 40, 8081-8087.

772 Querol, X., Alastuey, A., Orto, A., Pallares, M., Reina, F., Dieguez, J. J., Mantilla, E.,  
 773 Escudero, M., Alonso, L., Gangoiti, G., Millán, M., 2016. On the origin of the highest  
 774 ozone episodes in Spain. *Sci. Total Environ.*, 572, 379–389.

775 Reinhardt, T.E., Ottmar, R.D., Castilla, C., 2001. Smoke impacts from agricultural  
 776 burning in a rural Brazilian town. *J. Air Waste Manage. Assoc.*, 51, 443-450.

777 Riaño, D., Ruiz, J.A.M., Isidoro, D., Ustin, S.L., 2007. Spatial and temporal patterns of  
 778 burned area at global scale between 1981–2000 using NOAA-NASA Pathfinder. *Glob.*  
 779 *Change Biol.*, 13, 40-50.

780 Rosário, N. E., Longo, K. M., Freitas, S. R., Yamasoe, M. A., and Fonseca, R. M., 2013.  
 781 Modeling the South American regional smoke plume: aerosol optical depth variability  
 782 and Surface shortwave flux perturbation. *Atmos. Chem. Phys*, 13, 2923-2938.

783 Rousseeuw, P.J., 1987. Silhouettes: A graphical aid to the interpretation and validation of  
 784 cluster analysis. *Comput. Appl. Math.*, 20, 53-65.

785 Sarangi, T., Naja, M., Ojha, N., Kumar, R., Lal, S., Venkataramani, S., Kumar, A., Sagar,  
 786 R. and Chandola, H. C., 2014. First simultaneous measurements of ozone, CO, and  
 787 NO<sub>y</sub> at a high-altitude regional representative site in the central Himalayas, J.  
 788 *Geophys. Res. Atmos.*, 119, 1592–1611, doi:10.1002/2013JD020631.

789 Sillanpää, M, Saarikoski, S., Hillamo, R., Pennanen, A., Makkonen, U., Spolnik, Z., Van  
 790 Grieken, R., Koskentalo, T., Salonen, R.O., 2005. Chemical composition, mass size

791 distribution and source analysis of long-range transported wildfire smokes in Helsinki.  
 792 *Sci. Total Environ.*, 350, 119-135.

793 Škerlak, B., Sprenger, M., Wernli, H., 2014. A global climatology of stratosphere-  
 794 troposphere exchange using the ERA-Interim data set from 1979 to 2011. *Atmos.*  
 795 *Chem. Phys.*, 14, 913-937.

796 Stein, A.F., Draxler, R.R., Rolph, G.D., Stunder, B.J.B., Cohen, M.D., and Ngan, F., 2015.  
 797 NOAA's HYSPLIT atmospheric transport and dispersion modeling system, *Bull.*  
 798 *Amer. Meteor. Soc.*, 96, 2059-2077.

799 Targino, A.C., Krecl, P., 2016. Local and regional contributions to black carbon aerosols  
 800 in a mid-sized city in southern Brazil. *Aeros. Air Qual. Res.*, 16, 125-137.

801 Targino, A. C., Krecl, P., Johansson, C., Swietlicki, E., Massling, A., Coraiola, G. C.,  
 802 Lihavainen, H., 2013. Deterioration of air quality across Sweden due to transboundary  
 803 agricultural burning emissions. *Boreal Environ. Res.*, 18, 19-36.

804 Ten Hoeve, J.E., Remer, L.A., Correia, A.L., Jacobson, M.Z., 2012. Recent shift from  
 805 forest to savanna burning in the Amazon Basin observed by satellite. *Environ. Res.*  
 806 *Lett.*, 7, 1-8.

807 Torres-Jardon, R., and Keener, T.C., 2006. Evaluation of ozone-nitrogen oxides-volatile  
 808 organic compound sensitivity of Cincinnati, Ohio. *JAWMA*, 56, 322-333.

809 Vukovich, F.M., 2000. The spatial variation of the weekday/weekend differences in the  
 810 Baltimore area. *J. Air Waste Manage. Assoc.*, 50, 2067-2072.

811 Wentworth, G.R, Aklilu, Y., Landis, M.S., Hsu, Y.-M., 2018. Impacts of a large boreal  
 812 wildfire on ground level atmospheric concentrations of PAHs, VOCs and ozone.  
 813 *Atmos. Environ*, 178 19–30.



814 Wevers, M., De Fré, R., Desmedt, M., 2004. Effect of backyard burning on dioxin  
815 deposition and air concentrations. *Chemos.*, 54, 1351–1356.

816 Wilks, D. S., 2011. Statistical methods in the atmospheric sciences (3rd ed.). Oxford ;  
817 Waltham, MA: Academic Press.

818 Witham C., Manning A., 2007. Impacts of Russian biomass burning on UK air quality.  
819 *Atmos. Environ.*, 41, 8075-8090.

820 Zhou, Y., Luo, B., Li, J., Hao, Y., Yang, W., Shi, F., Chen, Y., Simayi, M., Xie, S., 2019.  
821 Characteristics of six criteria air pollutants before, during, and after a severe air  
822 pollution episode caused by biomass burning in the southern Sichuan Basin, China.  
823 *Atmos. Environ.*, 34, DOI:doi.org/10.1016/j.atmosenv.2019.116840.

824 Ziemke, J.R., Chandra, S., Labow, G.J., Bhartia, P.K., Froidevaux, L., Witte, J.C., 2011.  
825 A global climatology of tropospheric and stratospheric ozone derived from Aura OMI  
826 and MLS measurements. *Atmos. Chem. Phys.*, 11, 9237–9251.